Check for updates

Ion specific effects on the rheology of cellulose nanofibrils in the presence of salts†

Ravisara Wattana, [ID] [a] Daehwan Park[b] and Chinedum O. Osuji [ID] *[c]

Cellulose nanofibrils (CNFs) are high-aspect-ratio semiflexible filaments that can modify the rheology of fluids in which they are suspended. This work addresses the role of ionic strength in the rheology of CNF suspensions and the ion-specific nature of such rheology. Salt-free CNF suspensions exhibit viscoelastic, shear-thinning behavior. The concentration dependences of the storage modulus and specific viscosity exhibit similar power-law relationships in two regimes, $G' \sim \eta_{sp} \sim c^a$, with exponents of $a \approx 1$ and $a \approx 5$ below and above, respectively, a critical concentration of roughly 0.5 wt% that delineates "dilute" and "semi-dilute" characteristics. In the semi-dilute regime, salt addition increases the elastic modulus due to increased filament–filament association enabled by electrostatic screening of the repulsive interactions between weakly charged filaments. In the dilute regime, the intrinsic viscosity decreases with ionic strength, reflecting the adoption of more compact conformations at the single-filament level due to screened electrostatics. At a fixed ionic strength, both storage modulus and intrinsic viscosity show a marked dependence on ion identity, for which ion hydration enthalpy is used as a proxy. The storage modulus decreases with the enthalpy of hydration, whereas the intrinsic viscosity increases. Notably, the orderings of both parameters mimic the ion sequence of the Hofmeister series. This highlights a strong correlation between the ability of different ions to modify the hydrogen-bonding-network structure of water and their ability to screen inter- and intra-filament electrostatic interactions. This work provides new insight into ion-specific effects in CNF suspension rheology that can be used to rationally modify the properties of CNF-based complex fluids.

1. Introduction

Cellulosic nanomaterials such as cellulose nanofibrils (CNFs) and cellulose nanocrystals (CNCs) are versatile and useful materials in various contexts. Sourced from naturally abundant biomass, these materials can be chemically modified readily and are attractive from a sustainability perspective. These characteristics drive their use in applications ranging from traditional paper production to biomedical devices,[1–7] and the fabrication of a variety of functional hydrogels[8,9] and microcapsules.[10,11] They are also of interest for engineering complex fluids.[12,13] In particular, the high aspect ratio of CNFs makes it an effective rheology modifier at low volume fractions.[14,15] Chemical modification of cellulose by (2,2,6,

6-tetramethyl-piperidin-1-yl)oxyl (TEMPO) oxidation converts some fraction of hydroxyl groups to carboxylates (Fig. 1). At neutral pH, TEMPO-oxidized CNFs are weakly negatively charged, but otherwise hydrophobic materials.[16,17] At appropriate volume fractions, they form physical gel networks *via* electrostatic interactions and physical entanglement that are conceptually similar to polyelectrolyte gel networks[18] with intriguing yielding and aging responses.[19] Fig. 1 provides a schematic illustration of such a network. TEM and SEM images highlight the high aspect ratio and semi-flexible character of CNFs, here with diameters of 5.5 ± 1.4 nm and contour lengths exceeding 1000 nm. As with any other colloidal systems, the rheology of CNF suspensions is a function of inter-particle interactions, which can be modified by the addition of other species, including surfactants and dissociated ions from dissolved salts, polymers, or other colloids.[20–22]

From a generic perspective, the presence of dissolved salts in charged colloidal and macromolecular systems has significant implications for their rheological properties in aqueous media. Dissociated salt ions modify the electrostatic interactions between the colloidal and/or macromolecular components of a system, which leads to conformational changes, or changes in the state of aggregation, and concomitant modifications in the

[a] Department of Materials Science and Engineering, University of Pennsylvania, Philadelphia, Pennsylvania 19104, USA

[b] Department of Chemistry & Cosmetics, Jeju National University, 102 Jejudaehak-ro, Jeju-si, Jeju-do 63234, Republic of Korea

[c] Department of Chemical and Biomolecular Engineering, University of Pennsylvania, Philadelphia, Pennsylvania 19104, USA. E-mail: cosuji@seas.upenn.edu

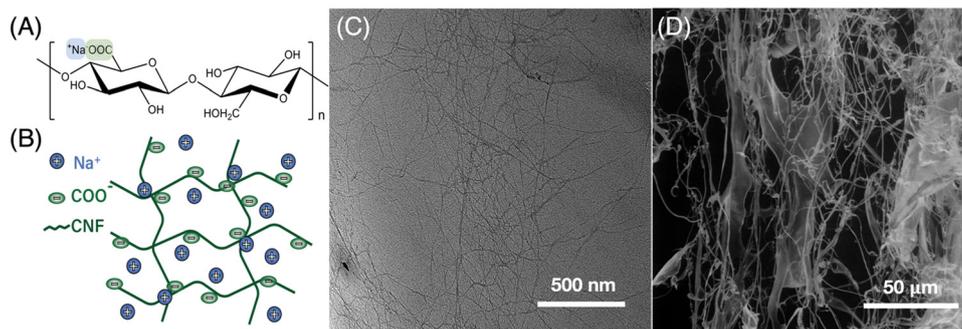† Electronic supplementary information (ESI) available. See DOI: https://doi.org/10.1039/d5sm00339c

Fig. 1 TEMPO-oxidized cellulose nanofibrils (CNFs): (A) chemical structure, (B) illustration of a three-dimensional network structure, (C) TEM image, and (D) SEM image.

rheology of the system. This is seen in polyelectrolyte complexes, for example, as shown in the alginate–chitosan system.[23] The presence of ionic species can have significant effects on the rheology of cellulose nanomaterials, with well-known impacts of ionic strength on physiochemical properties and behavior, manifested by solubility, dissolution, and aggregation,[24–26] conductivity and zeta-potential,[27,28] gelation,[29–35] and polymer adsorption.[36,37] Interestingly, unmodified CNFs are reported to be sensitive to the presence of salts at very small concentrations, $\sim$1 mM, despite the absence of charged or ionizable groups present on TEMPO-modified CNFs. The sensitivity has been linked to the effect of ions on the hydrogen bonding structure of water, and specifically, to the effect on CNF hydration, which thereby impacts the nature of fibril–fibril contacts.[38]

The strength and range of inter-particle interactions can be used to gauge the stability in colloidal suspensions by tallying contributions from electrostatic and dispersion forces.[39,40] Dissolved ions screen electrostatic interactions between charged colloidal particles due to the formation of electrical double layers. The modification to inter-particle potential is often described by the Derjaguin–Landau–Verwey–Overbeek (DLVO) theory, which considers the valency and concentration of ions. While DLVO theory is agnostic of ion identity, ion-specific effects were first introduced in protein dissolution as the conical example to understand the stability, or solubility, of proteins in aqueous media, as captured by the Hofmeister series (HS).[41–46] Such an effect has been subsequentially encountered in other systems, including gelatin,[47–52] collagen,[53] DNA,[54] polymer solutions,[55,56] polyelectrolyte films,[57] emulsions,[58] and nanoparticles.[59–62] As illustrated in Fig. 2, the HS describes the varying ability of different ions to stabilize or destabilize globular proteins in aqueous media. At a coarse level, this phenomenon has been linked to the order-inducing (kosmotropic) or disorder-inducing (chaotropic) effects of different ions on the water structure (and therefore on the hydrophobic effect) as primarily correlated with their charge density and therefore proxied by their hydrated radii and hydration enthalpies. The correlations are inverted for cations and anions – weakly hydrated cations and strongly hydrated anions are more chaotropic, whereas strongly hydrated cations and weakly hydrated anions are more kosmotropic. While this coarse-level description is useful in many scenarios, it sidesteps the role of
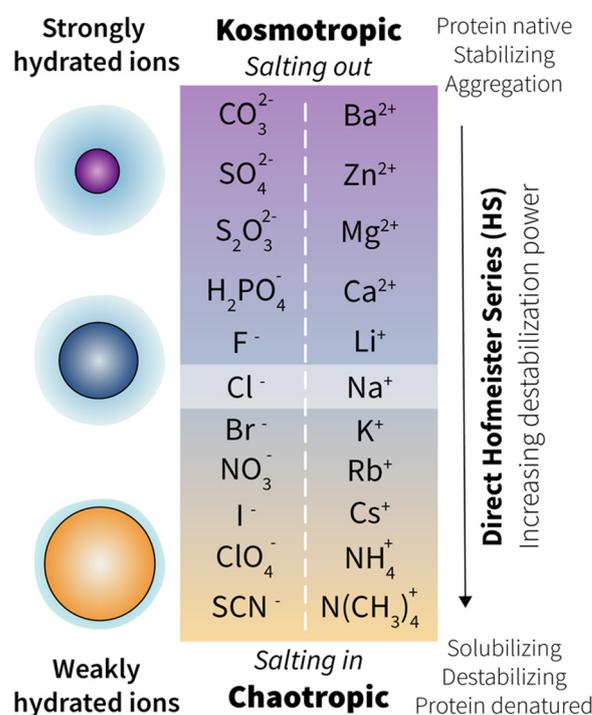

Fig. 2 Hofmeister series (HS), ion specificity series or lyotropic sequences for conventional protein precipitation.

non-additive and specific ion-solute interactions, counter-ion identity, protein charge, concentration dependence, and other contributions to ion-specific effects.[63–65] Nevertheless, it captures some important broad trends. For example, the lower charge density and greater polarizability of anions relative to cations lead to larger observable anion-specific effects, and studies regarding ion-specific effects more often focus on anion than cation identity.[65]

Here, we investigate the ion-specificity in terms of the effect of added salts on the rheology of TEMPO-oxidized aqueous CNF suspensions. Neat CNF suspensions display distinct dilute and semi-dilute regimes, separated by a critical concentration of roughly 0.5 wt%. Increasing the salt concentration leads to a decrease in intrinsic viscosity and an increase in gel modulus in the dilute and semi-dilute regimes, respectively. These changes

are due to screened electrostatic interactions which permit more compact single-filament conformations, and increased filament–filament contact, respectively. We study cation specific effects using a variety of chloride salts of monovalent cations in both the dilute and semi-dilute regimes. Clear trends emerge in both the dilute and semi-dilute regimes. The intrinsic viscosity decreases and storage modulus increases as it progresses along the Hofmeister series from kosmotropic to chaotropic cations. The storage modulus appears exponentially dependent on the enthalpy of hydration of the cation. We attribute these effects to the role of hydration shell-bound water in moderating the electrostatic screening that drives changes in filament conformation and association – larger hydration shells and tighter binding of waters limit the electrostatic interaction between the cation and the negatively charged carboxylate groups on CNFs, leading to a more diffuse double layer and less screening of electrostatic repulsion between CNFs. These findings highlight the non-trivial impact of ion identity in dictating the rheology of CNF suspensions and provide potential routes for optimizing the formulation of CNF-containing complex fluids.

2. Materials and methods

2.1 Sample preparation

All CNF samples were prepared from a stock 1.1 wt% aqueous suspension of (2,2,6,6-tetramethylpiperidin-1-yl)oxyl or TEMPO-modified CNF suspension obtained from the Process Development Center at the University of Maine. The CNF charge density is specified at 1.5 meq g^{-1} of dry material. Samples of varying compositions were prepared by either slowly concentrating the stock suspension using a rotary evaporator or diluting it with Milli-Q water, followed by vortex mixing. Nine chloride salts were examined to elucidate the monovalent and divalent cationic effects while four sodium salts were explored to probe the monovalent anion effect. All salts were obtained from Sigma-Aldrich as anhydrous high purity powders ($>99.99\%$, trace metals basis). The investigated monovalent chloride salts are lithium chloride (LiCl), sodium chloride (NaCl), potassium chloride (KCl), rubidium chloride (RbCl), and cesium chloride (CsCl). The sodium salts are sodium fluoride (NaF), sodium iodide (NaI), and sodium bromide (NaBr). The dichloride salts include magnesium chloride ($MgCl_2$), calcium chloride ($CaCl_2$), strontium chloride ($SrCl_2$), and barium chloride ($BaCl_2$). Stock solutions of 100 mM concentration were prepared by salt dissolution in Milli-Q water and diluted to desired concentrations. Salt-containing CNF samples were prepared by combining appropriate quantities and concentrations of CNF suspensions with salt solutions, followed by vortex mixing. Air bubbles were removed by gentle centrifugation at 1500 rpm for 5 minutes and left overnight quiescently before rheological measurements.

2.2 Characterization

Transmission electron microscopy (TEM). TEM imaging was performed using a JEM-F200 from JEOL with high resolution at a voltage of 200 kV and a cold emission source. A CNF suspension was diluted to 0.01 wt% and drop-cast onto a carbon film on a 200-mesh copper grid to prepare samples for imaging. Incubation of the TEM grid for 10 s by depositing a small drop (~ 5 µl) of 2 wt% uranyl acetate solution (Thomas Scientific) was used to enhance the contrast of the low electron density nanofibrils. The TEM sample was drained of excess stain solution, rinsed with DI water 1–2 times, and allowed to dry overnight under ambient conditions before the TEM characterization.

Scanning electron microscopy (SEM). The stock suspension was diluted with DI water to 0.02 wt% 10 ml of this 0.02 wt% suspension was placed in a centrifuge tube and freeze-dried by immersing the tube in liquid nitrogen, followed by water removal *via* lyophilization over 24 hours to obtain a dry, white, solid sample containing only nanofibers. SEM imaging was performed using the low vacuum mode of a TFS Quanta 600 environmental scanning electron microscope (ESEM) with a large field detector (LFD) at an accelerating voltage of 5 kV.

Rheological measurements. Rheological characterization was conducted using an Ubbelhode capillary viscometer for viscosity measurements and a strain-controlled rheometer for steady-flow and dynamic or oscillatory rheology. The capillary viscometer (UBC-0C, from Cannon Instrument Company, USA) is rated kinematic viscosity measurements ranging from 0.6 to 3.0 mm^2 s^{-1} and was calibrated by the supplier using ASTM D445 and ISO 3104 standards. Steady-flow curves, and strain-dependent and frequency-dependent dynamic measurements were conducted using an ARES G2 (TA Instruments, USA). For dilute neat CNF suspensions, the double-wall concentric cylinder (DWC) geometry was used to ensure sufficient torque generation by low viscosity samples relative to the noise floor of the instrument (100 nN m). Measurements of gels or high concentration suspensions were performed with a cone-and-plate geometry of 50 mm diameter and 0.04 rad cone-angle. Samples were thermostated at 20 °C and a thin layer of mineral oil was used at the sample–air interface to minimize water evaporation during the measurements. The samples were pre-sheared at 2 s^{-1} for 300 s and then left quiescently for another 300 s. Amplitude sweep measurements were conducted at $\omega = 10$ rad s^{-1} to determine the strain limit of the linear viscoelastic region (LVR) for the purpose of conducting frequency sweep measurements thereafter. An ascending strain sweep followed by a descending run was used to remove any sample history, prior to frequency dependent measurements. Frequency sweep measurements at strain amplitudes within the LVR were then performed, with ascending and descending ramps to verify data reproducibility.

3. Results and discussion

3.1 Viscoelasticity of neat CNF suspensions

At concentrations lower than 1.1 wt%, the neat CNF suspensions are viscoelastic fluids, with $G'' > G'$ over all observed frequencies. Above 1.1 wt%, they are more gel-like with $G' > G''$ and a largely frequency-independent elastic modulus, as seen in Fig. 3B. Full dynamic moduli of both amplitude and

frequency dependence are shown in Fig. 1S (ESI†). Flow curves (Fig. 3C) show a transition from purely Newtonian to shear-thinning behavior upon increasing the CNF concentration. Zero-shear viscosities, η_0, are obtained from fits of the data using the Cross model (eqn (1)).

$$\eta(\dot{\gamma}) = \eta_\infty + \frac{\eta_0 - \eta_\infty}{1 + (\lambda\dot{\gamma})^n} \qquad (1)$$

The concentration dependences of the storage modulus at $\omega = 10$ rad s^{-1} and the specific viscosity were examined, as shown in Fig. 4. The specific viscosity was calculated based on zero shear viscosities as $\eta_{sp} = (\eta_0 - \eta_s)/\eta_s$, where η_s is the viscosity of the solvent, *i.e.* water. The data reveal two distinct regimes of apparent power-law behavior, $G' \sim \eta_{sp} \sim c^a$. The exponent $a \approx 1$ at low concentrations and $a \approx 5$ at high concentrations, with a crossover at $c_c \approx 0.5$ wt%. The behavior in the semi-dilute regime, $c > c_c$, is broadly similar to that seen in prior work by Jowkarderis and van de Ven, who reported an exponent of 4.5 for elasticity measured at 6.28 rad s^{-1},[3] and by Pettersson *et al.*, who reported an exponent of 5.2, for carboxymethylated cellulose nanofibrils measured at roughly 0.1 rad s^{-1}.[66] It is worth noting, however, that a broad range of exponents have been observed in prior work[67] and that these exponents are typically larger than the 2–2.5 expected from classical theories for semi-flexible filamentous networks.[68] More recent work by Hill, however, suggests an exponent between 11/3 and 7.[69] The sensitivity of the measured storage modulus to the frequency in these weak gels results in a decrease in the concentration scaling exponent upon increasing the frequency. The use of moduli measured at different frequencies may account for some of the variation in reported exponents in the literature, beyond non-trivial effects due to differences associated with the degree of crystallinity, aspect ratio, and surface charge of variously sourced CNFs studied.

The linear concentration dependence of specific viscosity is expected in the dilute regime for any colloidal particle, independent of shape. At higher concentrations, hydrodynamic interactions give rise to exponents larger than unity. For our system, the exponent $a \approx 5$ is larger than would be expected for semiflexible
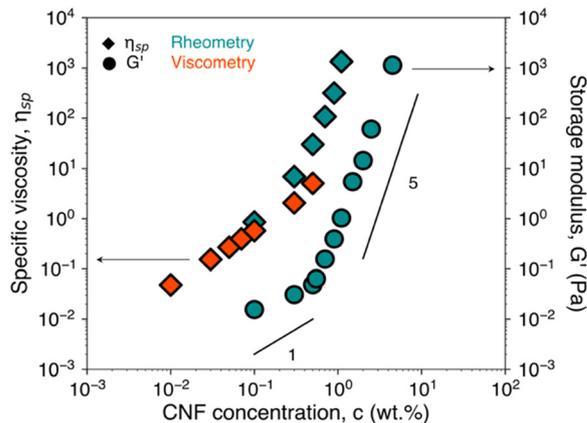

Fig. 4 CNF concentration dependence of specific viscosity and storage modulus of salt-free suspensions. Data in green and dark orange were collected from rheometric and viscometric measurements, respectively.

polymers below entanglement concentrations. We consider it likely that non-trivial filament–filament interactions (electrostatic repulsion; hydrophobic association) are responsible for the larger exponent. We are not aware of prior studies that address the concentration dependence of zero shear viscosity of CNFs in the semi-dilute regime. These can be somewhat challenging studies due to the difficulty of accurately measuring zero shear viscosities in this regime due to the onset of shear thinning at very low shear rates that preclude direct observation of the Newtonian plateau and, therefore, impose the need to fit rheometric data to extract the zero-shear viscosity. Concomitantly, viscometric experiments are prohibitively long. Nevertheless, we observe qualitatively good agreement between viscometric and rheometric data in the crossover region.

3.2 Viscoelasticity of CNF suspensions with NaCl

Fig. 5 shows images of 0.55 wt% CNF suspensions with various concentrations of NaCl ranging from 25 to 500 mM. For salt concentrations below 50 mM, the sample formed clear gels. At 50 mM, the gel formed was of sufficient strength to resist gravitational flow upon sample inversion (Fig. 5A). Above this
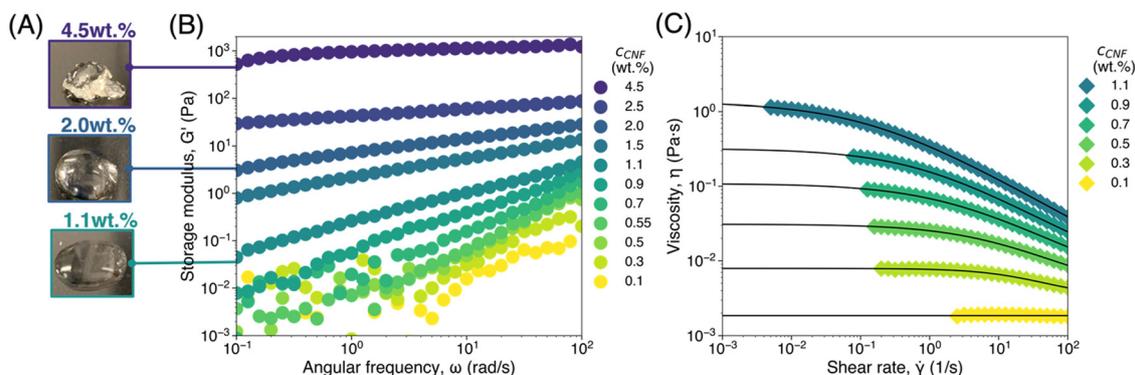

Fig. 3 (A) Photographs of CNF suspension samples at concentrations indicated. (B) Frequency dependent elastic moduli measured at a strain amplitude, $\gamma = 5\%$ for neat CNF suspensions of different concentrations (0.1 to 4.5 wt% as indicated). (C) Steady-flow curves of neat CNF suspensions (0.1 to 1.1 wt% as indicated). Solid lines are fits of the data using the Cross model (eqn (1)).

salt concentration, the suspensions become somewhat cloudy, and the gels lost their mechanical integrity. The results are consistent with an initial increase of modulus due to modest screening of electrostatic repulsion that enabled filament–filament interactions to form a stronger gel. However, excessive salt addition leads to gel collapse as stronger filament–filament association leads to flocculation and precipitation of aggregates. Our results highlight that there is a window within which an increase in ionic strength can modify the mechanical properties of CNF networks in a notably predictable fashion without causing large-scale aggregation and, therefore, without loss of optical clarity. Fig. 5C intriguingly shows exponential dependence of storage modulus on the salt concentration in the observed 0–50 mM NaCl range. This exponential dependence can be contrasted with linear[70] and logarithmic[71] dependences observed in other complex fluids. While the ionic strength dependence of gel modulus nominally originates in the reduction of longer range electrostatic repulsion and emergent relevance of short range van der Waals attraction as described by DLVO theory, in practice, the scaling of modulus with ionic strength is less straightforward to describe.

3.3 Intrinsic viscosity of CNFs in the presence of NaCl

We investigated the intrinsic viscosity of our CNFs using viscometric measurements in the dilute regime. The intrinsic viscosity ($[\eta]$ in eqn (2)) is the coefficient of proportionality that captures the ability of a particle to alter the suspension viscosity in relation to its concentration. It is therefore a direct function of the shape of the particle. For solid spherical particles, $[\eta] = 5/2$. Analytical and numerical results are available for short-fibers as a function of aspect ratio.[72] Particle shape can also correspond to intrinsic viscosity via packing efficiency as a function of aspect ratio.[73] For CNFs, prior work has shown that there is a direct correlation between the intrinsic viscosity and the aspect ratio,[74] and work by Isogai et al. suggested a correlation $\rho[\eta] \sim s^b$, where ρ and s are the mass density and aspect ratio, and $b \approx 1.9$.[75]

$$\eta_{red} = \frac{\eta_{sp}}{c} = \frac{\eta_r - 1}{c} = [\eta] + k_H[\eta]^2 c \qquad (2)$$

The concentration dependence of the reduced viscosity, $\eta_{red} = \eta_{sp}/c$, was linearly extrapolated to $c = 0$ to yield the intrinsic viscosity (Fig. 6A). The dependence of $[\eta]$ on the salt concentration, c_s, is shown in Fig. 6B. $[\eta]$ decreases by a factor of almost $3\times$ in going from neat CNF suspensions to 5 mM NaCl samples. There is no indication that salt addition shortens or otherwise alters the physical dimensions of CNFs, and so the aspect ratio, as strictly defined by the ratio of contour length to diameter, remains unchanged. A naïve interpretation in the context of the Isogai correlation therefore fails, necessarily. Recognizing that the preceding arguments do not incorporate the rigidity or conformational freedom of the CNF explicitly, i.e. separately from the aspect ratio, it is sufficient to recognize a change in the effective aspect ratio. We infer that, physically, the effective shape of CNFs has changed – a reduction in intrinsic viscosity is consistent with the adoption of a less
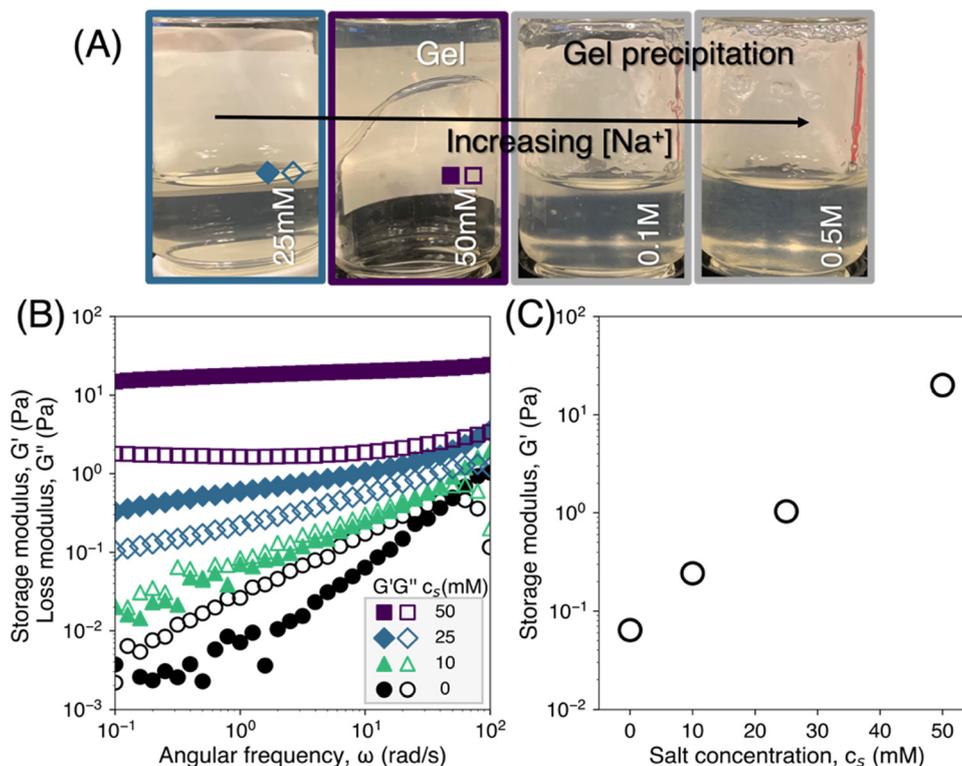

Fig. 5 (A) Photographs of CNF samples with varying salt concentrations. (B) Dynamic rheology of CNFs in the presence of NaCl at concentrations indicated. (C) NaCl concentration dependence of storage modulus at $\omega = 10$ rad s^{-1} for semi-dilute CNF suspensions.
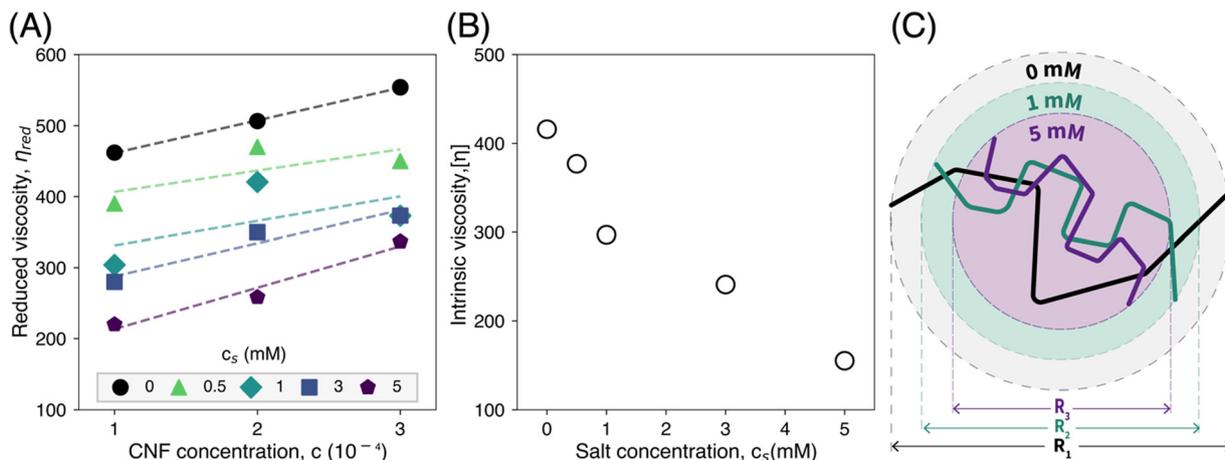
Fig. 6 (A) Reduced viscosity of dilute CNF suspensions as a function of CNF concentration, in the presence of NaCl at various concentrations, as indicated. (B) Corresponding intrinsic viscosities of CNFs as a function of NaCl concentration. (C) Schematic illustration of the change in the CNF shape due to the screening of electrostatic interactions. An increase in the salt concentration results in more compact configurations as the fibril is more flexible.

extended structure, which would likely result from screened electrostatics that liberate internal modes of motion in individual filaments. The zeta potential results, shown in Fig. 3S (ESI†), further support the reduction in screened electrostatics as more salt is added at a fixed CNF concentration. This is schematically illustrated in Fig. 6C. Effectively, the filament becomes less stiff. The reduction in the intrinsic viscosity on salt addition mirrors that seen in polyelectrolyte solutions on salt addition.[76]

The intrinsic viscosity of polyelectrolytes in solution displays sigmoidal dependence on the salt concentration.[77] This reflects a smooth transition from a low salt limit ($c_s = 0$) to a high salt limit ($c_s \rightarrow \infty$), at a characteristic salt concentration, or inflection point, c_s^{ip}, as shown in the Boltzman sigmoidal equation, eqn (3), where H is an adjustable scalar. Data and the corresponding fit are shown in Fig. 7(A). The upper limit ($[\eta] = 417$ ml g^{-1}) is the intrinsic viscosity of the CNF suspension in the absence of an additional salt.

$$\log[\eta] = \log[\eta]_{c_s \rightarrow \infty} + \frac{\log[\eta]_{c_s=0} - \log[\eta]_{c_s \rightarrow \infty}}{1 + e^{\log H(c_s/c_s^{ip})}} \qquad (3)$$

The ionic strength dependence can be modeled to yield information on the persistence length of the CNFs. The intrinsic viscosity of a polymer scales as the reciprocal of the overlap concentration, (c^*), which is the concentration within the pervaded volume, so $[\eta] \approx \frac{1}{c^*} \sim \frac{V}{M} = \Phi \frac{R^3}{M}$ where M is the mass of an individual chain in solution, Φ is a polymer specific numerical factor, and R is the root mean-square end–end distance which
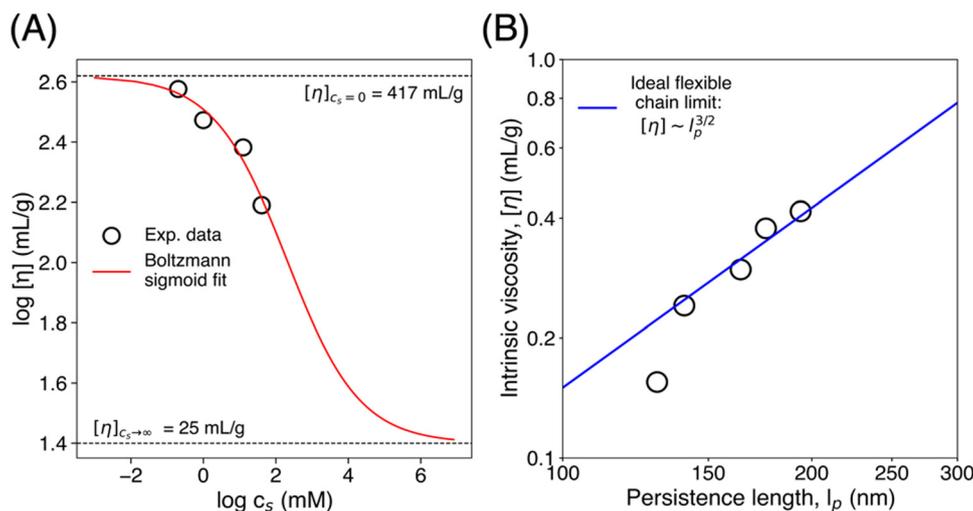

Fig. 7 (A) The logarithmic intrinsic viscosity dependence on the logarithmic values of salt concentrations. The solid line is the Boltzmann sigmoidal curve (eqn (3); $R^2 = 0.95$). (B) Intrinsic viscosity as a function of persistence length with a solid line indicating a 3/2 power-law as a visual guide. Persistence lengths were extracted from the WLC model fit (eqn (4) and (5)).

is directly proportional to the radius of gyration.[78] The mean square end–end distance for semi-flexible polymers is well represented by the worm-like chain (WLC) model as $\langle R^2 \rangle = 2l_p^2[L/l_p - (1 - es^{-L/l_p})]$. The WLC model provides a smooth interpolation between fully flexible, and fully rigid or rod-like polymer backbones corresponding to the limits $\frac{L}{l_p} \gg 1$ and $\frac{L}{l_p} = 1$ where L and l_p are the contour and persistence lengths, respectively. The intrinsic viscosity is therefore correlated with the chain persistence length as shown in eqn (4).

$$[\eta] \approx \bar{\Phi}[2l_p^2[L/l_p - (1 - e^{-L/l_p})]]^{3/2} \quad (4)$$

Models for the ionic strength dependence of persistence length include the well-known Odijk–Skolnick–Fixman (OSF) model[79,80] that suggests the form $l_p = A + B/I$ where $A = l_0$ is a minimum physical persistence length, and $l_e = B/I$ is an electrostatic screening length, $l_e = l_B/4A^2\kappa^2$ where l_B is the Bjerrum length, A is the charge density along the polymer, and κ is the Debye screening length. The interpolative model of Brunet and Manghi[81] (eqn (5)) provides additional tractability. It yields finite l_p at vanishing ionic strength, and a limiting power law dependence at high ionic strength, as observed experimentally. We use it here in combination with eqn (4) to examine the ionic strength dependence of intrinsic viscosity to determine the persistence length of CNFs. The results are shown in Fig. 7B. The persistence length varies over a limited range, from roughly 200 nm in salt-free suspensions to about 120 nm in 5 mM samples.

$$l_p = l_p^\infty + \frac{l_p^0 - l_p^\infty}{1 + (c_s/c_{s,0})^\delta} \quad (5)$$

3.4 Ion specific intrinsic viscosity of CNF suspensions

We examined the intrinsic viscosity of CNFs in the presence of various chloride salts, with different monovalent cations. The data are shown in Fig. 8. We observe that $[\eta]$ increases as we traverse a sequence of cations, from Cs^+ to Li^+ that inversely follows the Hofmeister series. Fig. 8B shows this dependence on ion-identity in terms of the enthalpy of hydration, with intrinsic viscosity increasing with the enthalpy of hydration. The data suggest that more extended CNF conformations are present for more strongly hydrated cations like Li^+. This dependence of conformation on hydration enthalpy is consistent with the expectation that more strongly hydrated cations are less effective in screening electrostatic interactions. This loss of effectiveness can be understood simply in terms of the ability or inability of hydrated ions to closely approach charged surfaces[82] such as the negatively charged CNF surface. An alternate way to view this is that close association of the ion with the charged surface requires a loss of water from the ion's hydration shell. Small, high charge-density and low polarizability species such as Li^+ distort the water structure more significantly and have larger hydrated diameters than larger, lower charge density species. Static light scattering experiments were unable to resolve statistically meaningful differences in the radius of gyration of CNFs in the presence of neighboring monovalent cations along the Hofmeister sequence. Data are shown in Table 2S and Fig. 4S (ESI†) with their 95% confidence intervals. The data, however, do show a statistically meaningful difference between the extracted radius of gyration of neat CNF and CNF/CsCl suspensions, i.e. corresponding to expected maximum and minimum dimensions from the intrinsic viscosity.

3.5 Ion specific viscoelasticity of CNF suspensions

Fig. 9(A) shows data from dynamic rheological characterization of CNF suspensions in the semi-dilute regime with 25 mM concentration of salts of varying identity. The suspensions are all soft gels and exhibit frequency dependence in their response, but with $G' > G''$ and, therefore, $\tan\delta < 1$ (Fig. 9B) over the observed frequency range. The storage modulus
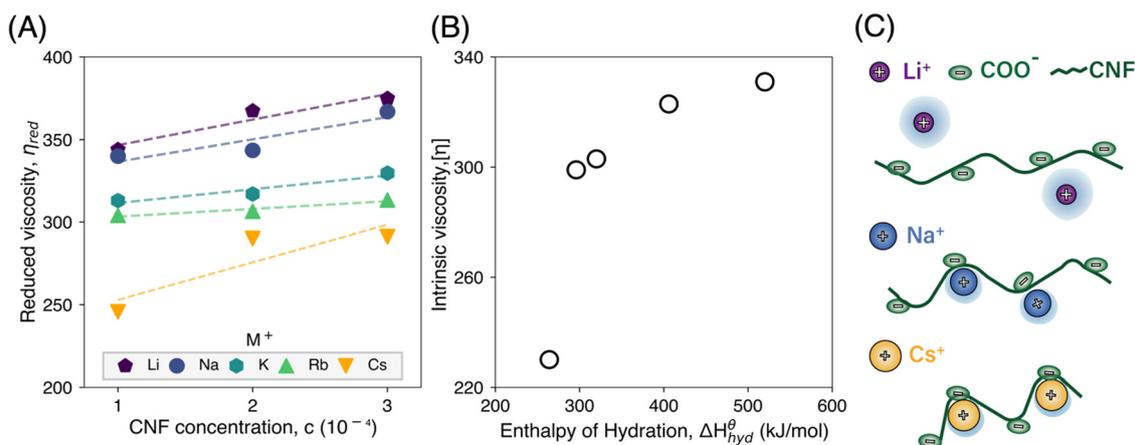

Fig. 8 (A) Reduced viscosity of dilute CNF suspensions as a function of CNF concentration, in the presence of chloride salts with the indicated monovalent cations. (B) Corresponding intrinsic viscosities of CNFs as a function of cation hydration enthalpy. The noted enthalpy of hydration values are tabulated and absolute values listed in Table 2S (ESI†).[83] (C) Schematic illustration of simplified representations of a change of a single CNF shape due to the ability to share or lose cations' hydration shells indicated in light blue borderlines on the ions.

decreases upon traversing the sequence from Cs^+ to Li^+, *i.e.* upon increasing the hydration enthalpy or ion charge density. As shown in Fig. 5, an increase in the concentration of a given salt (NaCl) leads to an increase of gel modulus, as screened electrostatic repulsion enables greater fibril–fibril association. We surmise that the decrease of modulus in Fig. 9 at a fixed salt concentration but changing ion identity (increasing hydration enthalpy) is associated with weaker inter-fibril association, or conversely, stronger repulsion due to decreased charge screening. This is consistent with the interpretation yielded from viscometry data, though the implications in terms of the measured quantities are different – a higher intrinsic viscosity, but a lower gel modulus. Fig. 9B shows that there is an apparent exponential dependence of the elastic modulus on the cation hydration enthalpy. This mirrors the exponential dependence of the gel modulus on the salt concentration seen in Fig. 5C for only NaCl presented. This suggests that the nominal ionic strength I can be corrected using the hydration enthalpy ΔH_h to yield an effective ionic strength, I_{eff}, that captures the role of salt addition agnostic of ion identity. Viewed another way, the difference in the effectiveness of electrostatic screening for ions of different charge densities can be accounted for by a term involving the hydration enthalpy, $G' \sim \exp[f(I, \Delta H_h)] = \exp[f(I_{eff})]$.

Fig. 9C displays Cole–Cole plots, *i.e.* the loss modulus $G'(\omega)$ as a function of the storage modulus $G'(\omega)$. The neat suspension exhibits near Maxwell type behavior as reflected in the semi-circular trace, $G''/G''_{max} = \sqrt{G'/G''_{max}(2 - G'/G''_{max})}$, where here the largest value G''_{max} is taken as characteristic of the system for this representation.[84,85] The 25 mM-salt-containing samples, however, display progressive departures from Maxwell behavior, with an increase in relaxation times and broadening of relaxation time distributions inferred, on going from Li^+ to Cs^+. Data are shown for additional salt concentrations in Fig. 2S (ESI†). Experiments conducted on a range of cations and anions

revealed a consistent correlation between the elastic modulus and the ion hydration enthalpy, with the modulus decreasing upon increasing the hydration enthalpy. This is seen in data shown in Fig. 10 for three investigated systems, *viz.* chloride salts (MCl), sodium salts (NaY), and dichloride salts (MCl$_2$), examining the effects of monovalent cations (M^+), monovalent anions (Y^-), and divalent cations (M^{2+}), respectively.

The ability of short-range ion solvation effects to alter colloidal interactions has been observed in a variety of systems, as described earlier. Work by van der Linden *et al.* examining the role of such non-DLVO effects on gelation of colloidal silica observed significant changes in gelation time for different monovalent cations, using simple inversion tests.[61] Gelation times were the longest for Li^+ and the shortest for Cs^+, with a strong power law dependence with the salt concentration. The effects were rationalized in terms of ion-specific hydration forces that dominate inter-particle interactions at length scales similar to those of the hydrated ions. The hydration forces represent energy barriers to particle association due to repulsion between structured water layers on or near particle surfaces, due to the hydrophilicity of the surface, or the presence of counterions. This effective hydration potential is a decreasing exponential function of particle separation and decreases with the salt concentration. Quantitative analysis of gelation times yielded estimates for the hydration potential and showed that the potential decreases in a sequence matching the Hofmeister series, but without a quantitative correlation with potentially relevant characteristics of the ionic species, such as hydration enthalpy. These arguments are broadly consistent with our observations – suppression of inter-particle interactions by strongly hydrated species can be seen as a consequence of reduced electrostatic screening.

4. Conclusion

In summary, we examined the behavior of CNF suspensions in water using a combination of viscometry and dynamic shear
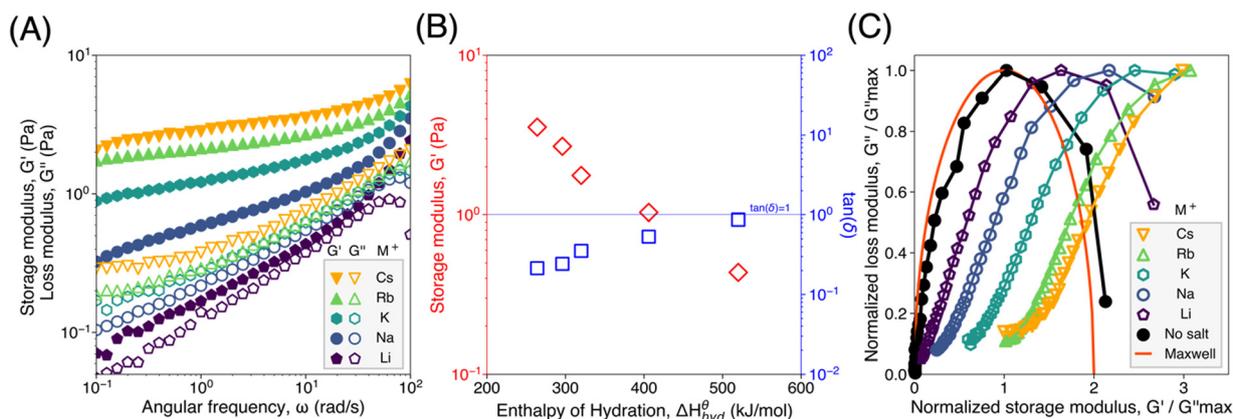

Fig. 9 (A) Dynamic rheology of CNFs in the presence of chloride salts with indicated monovalent cations at 25 mM. (B) Hydration enthalpy dependence on storage modulus (G': ◇) and loss factor (tan δ: □) at $w = 10$ rad s^{-1}. The noted enthalpy of hydration is tabulated and absolute values listed in Table 2S (ESI†).[82] (C) Cole–Cole plot of the CNF dynamic modulus in the absence and the presence of chloride salts with indicated monovalent cations at 25 mM. The solid line represents an ideal Maxwell fluid, a fluid with a single relaxation time, for which $G''/G''_{max} = \sqrt{G'/G''_{max}(2 - G'/G''_{max})}$ where G''_{max} is a characteristic modulus for the system.
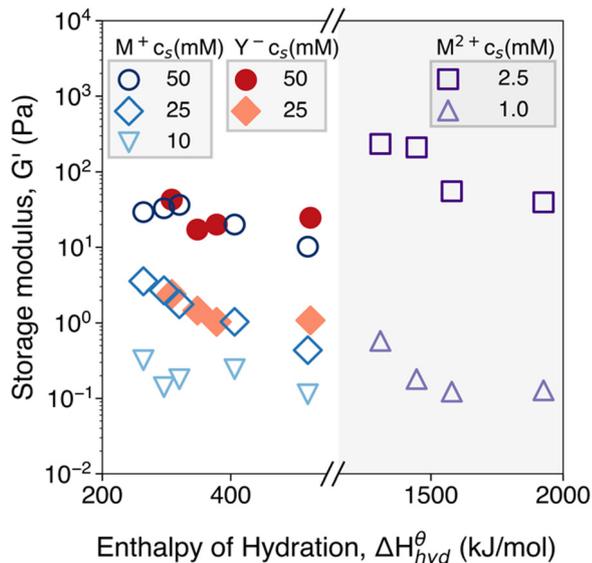
Fig. 10 Hydration enthalpy dependence of chloride salts (MCl) with monovalent cations (M^+: ○ 50 mM, ◇ 25 mM, ▽ 10 mM), sodium salts (NaY) with monovalent anions (Y^-: ● 50 mM, ◆ 25 mM), and dichloride salts (MCl_2) with divalent cations (M^{2+}: □ 2.5 mM, △ 1.0 mM) on the storage modulus of CNF suspensions. The storage moduli were extracted from the frequency sweep measurements in the LVR at ω = 10 rad s^{-1}. The enthalpy of hydration values are tabulated and absolute values are obtained from W. E. Dasent's Inorganic Energetics.[82]

rheology measurements. At very low concentrations of 0.1 wt% the suspensions appear Newtonian across the range of shear rates considered but exhibit shear thinning at progressively lower shear rates for concentrations in excess of this value. Similarly, the suspensions are viscoelastic fluids at low concentrations, and viscoelastic solids at high concentrations. The concentration dependence of zero shear viscosity and shear moduli establishes a transition from dilute to semi-dilute behavior at around a critical concentration of 0.5 wt%. Addition of NaCl to suspensions in the dilute regime resulted in a decrease in intrinsic viscosity. For suspensions in the semi-dilute regime, NaCl addition results in the formation of clear, uniform gels up to a concentration as high as 50 mM, beyond which CNF aggregation resulted in heterogeneous and opaque samples. The gels show an exponential dependence of elastic modulus on the salt concentration over the range in which clear, uniform gels were observed. These results are consistent with the screening of electrostatic interactions between CNFs that leads to the adoption of more compact conformations of individual CNFs in dilute solution and fibril–fibril association in the semi-dilute regime, leading to a reduction of intrinsic viscosity and persistence length, and an increase in elastic modulus, respectively.

The response of CNF suspensions to salt addition showed clear dependence on ion identity. At a given salt concentration, the intrinsic viscosity increases, and the gel modulus decreases, for variation of monovalent cations from a low to high charge density, *i.e.* from Cs$^+$ to Li$^+$, in direct accordance with the Hofmeister sequence. This demonstrates that the efficacy of

electrostatic screening is tightly coupled to the ion identity. These effects are well correlated with ion hydration enthalpies, and remarkably, the elastic modulus shows a clear decreasing exponential dependence on absolute hydration enthalpy. It suggests that the decrease in electrostatic screening by higher charge density species may be rationalized in terms of an effective ionic strength leading to $G' \sim \exp[f(I, \Delta H_h)] = \exp[f(I_{eff})]$. These results shed new light on the manner in which electrostatic screening governs the conformation and rheology of CNFs in suspensions and have potentially significant implications for the design and optimization of complex fluids and materials containing CNFs. The observed concentration-dependent behavior of CNF suspensions, coupled with the impact of salt addition on electrostatic screening, can be leveraged in applications such as drug delivery, food, cosmetics, and coatings, where the rheological properties of suspensions are crucial. The ability to control CNF conformation and fibril–fibril interactions *via* the salt concentration and ion identity could enable the tailoring of material properties for specific uses, such as creating uniform gels with controlled elasticity or enhancing the stability and flow behavior of suspensions in diverse formulations.

Data availability

The data supporting this article have been included as part of the ESI.†

Conflicts of interest

The authors declare no conflicts of interest.

Acknowledgements

References

1 T. Heinze, O. A. El Seoud and A. Koschella, Cellulose Derivatives: Synthesis, Structure, and Properties, *Springer Series on Polymer and Composite Materials (SSPCM)*, Springer, 2018, DOI: 10.1007/978-3-319-73168-1.

2 L. Jowkarderis and T. G. M. van de Ven, *Cellulose*, 2014, **21**, 2511–2517.

3 L. Jowkarderis and T. G. M. van de Ven, *Carbohydr. Polym.*, 2015, **123**, 416–423.

4 D. Miyashiro, R. Hamano and K. Umemura, *Nanomaterials*, 2020, **10**, 186.

5 C. Salas, T. Nypelö, C. Rodriguez-Abreu, C. Carrillo and O. J. Rojas, *Curr. Opin. Colloid Interface Sci.*, 2014, **19**, 383–396.

6 A. K. Mohanty, M. Misra and L. T. Drzal, *J. Polym. Environ.*, 2002, **10**, 19–26.

7 D. Klemm, B. Heublein, H. P. Fink and A. Bohn, *Angew. Chem., Int. Ed.*, 2005, **44**, 3358–3393.

8 D. Park, J. W. Kim and C. O. Osuji, *ACS Appl. Eng. Mater.*, 2024, **2**, 772–780.

9 D. Park, C. O. Osuji and J. W. Kim, *Small Methods*, 2023, **7**, 2201195.

10 A. P. Dhand, R. Poling-Skutvik and C. O. Osuji, *Soft Matter*, 2021, **17**, 4517–4524.

11 G. Kaufman, S. Mukhopadhyay, Y. Rokhlenko, S. Nejati, R. Boltyanskiy, Y. Choo, M. Loewenberg and C. O. Osuji, *Soft Matter*, 2017, **13**, 2733–2737.

12 M. C. Li, X. Y. Liu, K. H. Lv, J. S. Sun, C. L. Dai, B. Liao, C. Z. Liu, C. T. Mei, Q. L. Wu and M. Hubbe, *Prog. Mater. Sci.*, 2023, **139**, 101187.

13 M. A. Khan, K. Lv, J. S. Sun, H. K. Shen, Y. X. Zhang, A. A. Noor, S. M. Lalji, C. Z. Liu and M. C. Li, *Geoenergy Sci. Eng.*, 2025, **244**, 213524.

14 X. X. Sun, Q. L. Wu, S. Lee, Y. Qing and Y. Q. Wu, *Sci. Rep.*, 2016, **6**, 31654.

15 N. Quennouz, S. M. Hashmi, H. S. Choi, J. W. Kim and C. O. Osuji, *Soft Matter*, 2016, **12**, 157–164.

16 A. Isogai, T. Saito and H. Fukuzumi, *Nanoscale*, 2011, **3**, 71–85.

17 T. Saito, S. Kimura, Y. Nishiyama and A. Isogai, *Biomacromolecules*, 2007, **8**, 2485–2491.

18 S. F. Souza, M. Mariano, M. A. De Farias and J. S. Bernardes, *J. Colloid Interface Sci.*, 2019, **538**, 228–236.

19 R. Poling-Skutvik, E. McEvoy, V. Shenoy and C. O. Osuji, *Phys. Rev. Mater.*, 2020, **4**, 102601(R).

20 M. A. Hubbe, P. Tayeb, M. Joyce, P. Tyagi, M. Kehoe, K. Dimic-Misic and L. Pal, *BioResources*, 2017, **12**, 9556–9661.

21 A. I. Koponen, *Cellulose*, 2020, **27**, 1879–1897.

22 M. C. Li, Q. L. Wu, R. J. Moon, M. A. Hubbe and M. J. Bortner, *Adv. Mater.*, 2021, **33**, 21.

23 A. Varadarajan, L. T. Kearney, J. K. Keum, A. K. Naskar and S. Kundu, *Biomacromolecules*, 2023, **24**, 2730–2740.

24 Z. J. Liu, C. Zhang, R. G. Liu, W. S. Zhang, H. L. Kang, P. P. Li and Y. Huang, *Cellulose*, 2016, **23**, 295–305.

25 T. Phan-Xuan, A. Thuresson, M. Skepö, A. Labrador, R. Bordes and A. Matic, *Cellulose*, 2016, **23**, 3653–3663.

26 T. C. Cao and M. Elimelech, *J. Colloid Interface Sci.*, 2021, **584**, 456–463.

27 S. Shafiei-Sabet, W. Y. Hamad and S. G. Hatzikiriakos, *Cellulose*, 2014, **21**, 3347–3359.

28 A. Wang, Z. Y. Yuan, C. P. Wang, L. M. Luo, W. F. Zhang, S. Geng, J. L. Qu, B. Wei and Y. B. Wen, *Biomacromolecules*, 2020, **21**, 1471–1479.

29 N. Almeida, L. Rakesh and J. Zhao, *Food Hydrocolloids*, 2014, **36**, 323–331.

30 N. Almeida, L. Rakesh and J. Zhao, *Carbohydr. Polym.*, 2014, **99**, 630–637.

31 N. Mittal, T. Benselfelt, F. Ansari, K. Gordeyeva, S. V. Roth, L. Wågberg and L. D. Söderberg, *Angew. Chem., Int. Ed.*, 2019, **58**, 18562–18569.

32 L. Valencia, E. M. Nomena, S. Monti, W. Rosas-Arbelaez, A. P. Mathew, S. Kumar and K. P. Velikov, *Nanoscale*, 2020, **12**, 15652–15662.

33 K. M. Z. Hossain, V. Calabrese, M. A. da Silva, S. J. Bryant, J. Schmitt, J. H. Ahn-Jarvis, F. J. Warren, Y. Z. Khimyak, J. L. Scott and K. J. Edler, *Polymers*, 2021, **13**, 951.

34 Y. Song, B. Kim, J. D. Park and D. J. Lee, *Carbohydr. Polym.*, 2023, **300**, 120262.

35 K. Kobayashi, N. Isobe, R. Kusumi, J. Nemoto and M. Wada, *Biomacromolecules*, 2024, **25**, 864–870.

36 V. Arumughan, H. D. Özeren, M. Hedenqvist, M. Skepö, T. Nypelö, M. Hasani and A. Larsson, *Langmuir*, 2023, **39**, 15014–15021.

37 V. Arumughan, T. Nypelö, M. Hasani, H. Brelid, S. Albertsson, L. Wågberg and A. Larsson, *Colloids Surf., A*, 2021, **626**, 127006.

38 S. Arola, Z. N. Kou, B. J. M. Rooijakkers, R. Velagapudi, M. Sammalkorpi and M. B. Linder, *Cellulose*, 2022, **29**, 6109–6121.

39 C. A. S. Batista, R. G. Larson and N. A. Kotov, 2015, **350**.

40 M. Boström, D. R. M. Williams and B. W. Ninham, *Phys. Rev. Lett.*, 2001, **87**, 168103.

41 M. Lund, P. Jungwirth and C. E. Woodward, *Phys. Rev. Lett.*, 2008, **100**, 258105.

42 H. I. Okur, J. Hladílková, K. B. Rembert, Y. Cho, J. Heyda, J. Dzubiella, P. S. Cremer and P. Jungwirth, *J. Phys. Chem. B*, 2017, **121**, 1997–2014.

43 J. R. Feng, Y. Zhao, L. Z. Jiang, Y. Zhang and X. N. Sui, *Food Hydrocolloids*, 2024, **149**, 109577.

44 Y. X. Liu, X. Y. Li, J. M. Liu, L. K. Wei, Y. H. Liu, F. P. Lu, W. H. Wang, Q. G. Li and Y. Li, *Food Hydrocolloids*, 2022, **133**, 107976.

45 Y. Q. Lei, H. Ouyang, W. Peng, X. W. Yu, L. Jin and S. G. Li, *Gels*, 2022, **8**, 259.

46 Y. H. Cho, Y. J. Zhang, T. Christensen, L. B. Sagle, A. Chilkoti and P. S. Cremer, *J. Phys. Chem. B*, 2008, **112**, 13765–13771.

47 C. D. Qiao, J. L. Zhang, X. G. Ma, W. L. Liu and Q. Z. Liu, *Int. J. Biol. Macromol.*, 2018, **107**, 1074–1079.

48 V. Ball, *J. Phys. Chem. B*, 2019, **123**, 8405–8410.

49 B. H. Wu, M. Siglreitmeier, C. Debus, D. Schwahn, H. Cölfen and V. Pipich, *Macromol. Biosci.*, 2018, **18**, 1800018.

50 X. J. Wang, C. D. Qiao, K. Song, S. Jiang and J. S. Yao, *Colloids Surf., B*, 2021, **206**, 111944.

51 X. J. Wang, C. D. Qiao, S. Jiang, L. B. Liu and J. S. Yao, *Colloids Surf., B*, 2022, **217**, 112674.

52 S. Das, L. Giri and S. Majumdar, *Eur. Polym. J.*, 2023, **189**, 111961.

53 A. M. Oechsle, M. Landenberger, M. Gibis, S. B. Irmscher, R. Kohlus and J. Weiss, *Int. J. Biol. Macromol.*, 2015, **79**, 518–526.

54 S. Cruz-León, W. Vanderlinden, P. Müller, T. Forster, G. Staudt, Y. Y. Lin, J. Lipfert and N. Schwierz, *Nucleic Acids Res.*, 2022, **50**, 5726–5738.

55 K. Sakota, D. Tabata and H. Sekiya, *J. Phys. Chem. B*, 2015, **119**, 10334–10340.

56 S. Z. Moghaddam and E. Thormann, *J. Colloid Interface Sci.*, 2019, **555**, 615–635.

57 T. Klacic, K. Bohinc and D. Kovacevic, *Macromolecules*, 2022, **55**, 9571–9582.

58 J. C. Courtenay, Y. Jin, J. Schmitt, K. M. Z. Hossain, N. Mahmoudi, K. J. Edler and J. L. Scott, *Langmuir*, 2021, **37**, 6864–6873.

59 T. Oncsik, G. Trefalt, M. Borkovec and I. Szilagyi, *Langmuir*, 2015, **31**, 3799–3807.

60 C. Kaulen and U. Simon, *RSC Adv.*, 2018, **8**, 1717–1724.

61 M. van der Linden, B. O. Conchuir, E. Spigone, A. Niranjan, A. Zaccone and P. Cicuta, *J. Phys. Chem. Lett.*, 2015, **6**, 2881–2887.

62 C. Sögaard, K. Kolman, M. Christensson, A. B. Otyakmaz and Z. Abbas, *Colloids Surf., A*, 2021, **611**, 125872.

63 W. Kunz, *Curr. Opin. Colloid Interface Sci.*, 2010, **15**, 34–39.

64 A. Salis and B. W. Ninham, *Chem. Soc. Rev.*, 2014, **43**, 7358–7377.

65 B. B. Kang, H. C. Tang, Z. D. Zhao and S. S. Song, *ACS Omega*, 2020, **5**, 6229–6239.

66 A. Naderi, T. Lindström and T. Pettersson, *Cellulose*, 2014, **21**, 2357–2368.

67 O. Nechyporchuk, M. N. Belgacem and F. Pignon, *Biomacromolecules*, 2016, **17**, 2311–2320.

68 F. C. Mackintosh, J. Kas and P. A. Janmey, *Phys. Rev. Lett.*, 1995, **75**, 4425–4428.

69 R. J. Hill, *Biomacromolecules*, 2008, **9**, 2963–2966.

70 P. Schexnailder, E. Loizou, L. Porcar, P. Butler and G. Schmidt, *Phys. Chem. Chem. Phys.*, 2009, **11**, 2760–2766.

71 Y. Feng, M. Taraban and Y. B. Yu, *Soft Matter*, 2012, **8**, 11723–11731.

72 W. Pabst, E. Gregorová and C. Berthold, *J. Eur. Ceram. Soc.*, 2006, **26**, 149–160.

73 S. Mueller, E. W. Llewellin and H. M. Mader, *Geophys. Res. Lett.*, 2011, **38**, L13316.

74 S. Iwamoto, S.-H. Lee and T. Endo, *Polym. J.*, 2014, **46**, 73–76.

75 R. Tanaka, T. Saito, H. Hondo and A. Isogai, *Biomacromolecules*, 2015, **16**, 2127–2131.

76 B. E. Conway, *J. Polym. Sci.*, 1955, **18**, 257–274.

77 A. Eich and B. A. Wolf, *ChemPhysChem*, 2011, **12**, 2786–2790.

78 M. Rubinstein and R. H. Colby, *Polymer physics*, Oxford University Press, Oxford, New York, 2003.

79 T. Odijk, *J. Polym. Sci., Polym. Phys. Ed.*, 1977, **15**, 477–483.

80 J. Skolnick and M. Fixman, *Macromolecules*, 1977, **10**, 944–948.

81 A. Brunet, C. Tardin, L. Salomé, P. Rousseau, N. Destainville and M. Manghi, *Macromolecules*, 2015, **48**, 3641–3652.

82 K. P. Gregory, G. R. Elliott, H. Robertson, A. Kumar, E. J. Wanless, G. B. Webber, V. S. J. Craig, G. G. Andersson and A. J. Page, *Phys. Chem. Chem. Phys.*, 2022, **24**, 12682–12718.

83 W. E. Dasent, *Inorganic energetics: an introduction*, Cambridge University Press, Cambridge, 2nd edn, 1970.

84 D. J. Bischoff, T. Lee, K. S. Kang, J. Molineux, W. O. Parker, J. Pyun and M. E. Mackay, *Nat. Commun.*, 2023, **14**, 7553.

85 J. K. Song, N. Holten-Andersen and G. H. Mckinley, *Soft Matter*, 2023, **19**, 7885–7906.